Nano Research Energy

ISSN 2791-0091 (print); 2790-8119 (online)
https://doi.org/10.26599/NRE.2024.9120110

Research Article

Hybrid hydrovoltaic electricity generation driven by water evaporation

Xuemei Li[1,2] (✉), Gu Feng[2], Yiding Chen[1,3], Jidong Li[1], Jun Yin[1,3], Wei Deng[1] (✉), and Wanlin Guo[1,3] (✉)

[1] *State Key Laboratory of Mechanics and Control of Mechanical Structures, Key Laboratory for Intelligent Nano Materials and Devices of the Ministry of Education, Institute for Frontier Science, Nanjing University of Aeronautics and Astronautics, Nanjing 210016, China*
[2] *College of Material Science and Engineering, Nanjing University of Aeronautics and Astronautics, Nanjing 210016, China*
[3] *College of Aerospace Engineering, Nanjing University of Aeronautics and Astronautics, Nanjing 210016, China*

Received: 3 November 2023 / **Revised:** 28 November 2023 / **Accepted:** 29 November 2023

ABSTRACT

Water evaporation is a ubiquitous natural process exploiting thermal energy from ambient environment. Hydrovoltaic technologies emerged in recent years offer one prospective route to generate electricity from water evaporation, which has long been overlooked. Herein, we developed a hybrid hydrovoltaic generator driven by natural water evaporation, integrating an "evaporation motor" with an evaporation-electricity device and a droplet-electricity device. A rotary motion of the "evaporation motor" relies on phase change of ethanol driven by water-evaporation induced temperature gradient. This motion enables the evaporation-electricity device to work under a beneficial water-film operation mode to produce output of ~4 V and ~0.2 μA, as well as propels the droplet-electricity device to convert mechanical energy into pulsed output of ~100 V and ~0.2 mA. As different types of hydrovoltaic devices require distinctive stimuli, it was challenging to make them work simultaneously, especially under one single driving force. We here for the first time empower two types of hydrovoltaic devices solely by omnipresent water evaporation. Therefore, this work presents a new pathway to exploiting water evaporation-associated ambient thermal energy and provides insights on developing hybrid hydrovoltaic generators.

KEYWORDS

hybrid hydrovoltaic generator, ambient thermal energy, evaporation motor, water evaporation

1 Introduction

The natural water cycle, also known as the hydrologic cycle, describes the continuous movement and phase change of water on earth, in the form of physical processes of evaporation, transpiration, condensation, precipitation, infiltration, surface runoff and subsurface flow. Tremendous energy is contained in this global water cycle and hydroelectric power plants have been prevailed through the whole industrial era to harvest potential energy from large water reservoirs [1]. However, the energy involved in other processes, such as evaporation, raining, waving, and moisture, has long been left largely untapped due to the lack of energy conversion technologies fit for those processes. The last decade has been embracing the emergence of hydrovoltaic technologies, which allow for the harvesting of almost full energy spectrum of the water cycle and hold great potential to advance energy diversification, promoting the contribution of sustainable energy in particular [2, 3].

Hydrovoltaic technologies consist of three main types of energy conversion mechanisms and corresponding device configurations, targeting at water evaporation, water movement (including waving, raining and droplet moving), and moisture. Electricity is generated upon water infiltrating in a porous matrix driven by evaporation, wherein abundant nanochannels separate ions selectively to produce streaming potential and water evaporating at the capillary front induces evaporating potential [4–7]. It has been receiving tremendous attention since the first report [4] and intensive research efforts have been devoted to enhance the output performance by materials development [8–20], surface functionalization [21] and thermal management [22, 23]. We recently discovered the pivotal role of capillary front, by broadening which we obtained a ~5 V output of a single unit, much higher than previously reported results, and achieved integrated kilovolt level output in a water-film operation mode [24]. Water droplet and waving induced electricity was firstly found on monolayer graphene [25–27], termed as drawing potential and waving potential, and then revives in fluoropolymers (e.g., PTFE and FEP) based systems for rain droplets and water flowing in tubes involving bulk effect [28–36]. Moisture-based electricity generation converts chemical potential energy derived from moisture diffusion when water molecules contact with hydroscopic materials [37]. Years of relevant research efforts have

Address correspondence to Xuemei Li, xmli@nuaa.edu.cn; Wei Deng, weideng@nuaa.edu.cn; Wanlin Guo, wlguo@nuaa.edu.cn

committed to realizing continuous electricity generation and high integrated output voltage from moisture-electric devices [37–41].

Viewing from the aspect of spatiotemporal distribution, water evaporation is more ubiquitous than water movement; the latter is closely dependent on weather and geography. However, as the aforementioned hydrovoltaic devices respond to different stimuli, it is challenging to exploit water evaporation as the sole and omnipresent driving force for hybrid hydrovoltaic devices in order to acquire improved output. Our recent work revealed that a preformed water film, produced by periodically immersing the porous film in water, could promote the water-evaporation-induced electricity by one order of magnitude [24]. This water film process involves periodic mechanical movement, similar to what is required for water-droplet-based electricity generation. Therefore, one possible hybrid device is what is able to initiate mechanical motion and drive both water-evaporation and droplet-based electricity generation.

In this work, we developed a hybrid hydrovoltaic generator solely driven by omnipresent water evaporation. The hybrid generator consists of a self-floating "drinking-bird" like heat engine, termed as "evaporation motor", that converts evaporation-induced temperature difference to periodic rotation. The water-evaporation-based and droplet-based electricity generation devices were integrated with the self-floating heat engine of induced mechanical motion to augment water-evaporation-induced-electricity to an output of ~4 V and initiate droplet-based generator to produce an instantaneous output of ~100 V. The hybrid device with power management circuits could effectively charge capacitors and power a liquid crystal display. This work expands the applications of water-evaporation-relevant hydrovoltaic technologies and offers a new routine to hybrid hydrovoltaic devices with promoted output performance.

2 Results and discussion

2.1 Water evaporation driven periodic rotation

Electricity generation from both evaporation operated at the water-film mode [24] and water flowing in fluoropolymer tubes [31, 32] requires periodic relative motion between water and the solid surface. Therefore, we first design a self-floating "drinking bird" like heat engine that can rotate periodically solely driven by water evaporation, which we term as a "evaporation motor" (Fig. 1). The fabrication process is illustrated in Fig. S1 in the Electronic Supplementary Material (ESM). The "evaporation motor" consists of two glass bulbs joined by a plastic tube and the bottom bulb is filled with a certain amount of ethanol. The tube extends nearly all the way into the bottom bulb, and attaches to the top bulb. A hypodermic needle connected with a check valve is inserted into the plastic tube to facilitate evacuating the gas (mainly air) inside the bulbs so that the interior pressure of the top bulb is sensitive to the surface temperature of the top bulb. The top bulb with a "beak" is cover by air-laid paper to wick water and lower surface temperature by evaporation. The unit is then supported on a cylindrical plastic jar to make the "evaporation motor" self-floating and able to rotate with low friction. A weight and polyethylene foam are added to adjust the rotation dynamics (Fig. 1(b)).

The "evaporation motor" is fundamentally a heat engine that relies on temperature difference to initiate rotary motion. Due to the high enthalpy of vaporization of water (~ 2440 kJ/kg at 25 °C), water evaporation lowers the surface temperature of the air-laid paper covered on the top bulb to 22 °C, which was 4 °C lower than that of the bottom bulb (Fig. 1(c)). Resultantly, ethanol vapor inside the top bulb tends to condense on the interior cool surface, decreasing the number of ethanol gas molecules therein. According to the ideal gas law, $pV = Nk_BT$, where p, V, N, k_B, T are the pressure, volume, number of particles, Boltzmann constant, and temperature respectively, reduction of the ethanol gas molecules leads to a pressure drop in the top bulb (Fig. 1(d)). The pressure difference between the bottom and top bulb then pumps liquid ethanol from the bottom bulb up to the tube and top bulb. The gravitational center shifts towards up right accordingly, causing a clockwise torque M, and the device starts to rotate. Once the bottom end of the tube rises above the surface of liquid ethanol in the bottom bulb, a bubble of warm ethanol vapor rises up in the tube and displaces liquid ethanol, i.e., pressure equalizes between the bottom and top bulbs, and liquid ethanol in the tube and the top bulb flows back the bottom bulb. Though the torque at this moment switches from clockwise to counter-clockwise, the device continues rotating clockwise because of inertia since at this moment the device still possesses a clockwise angular velocity. The device rotates clockwise until the "beak" on the top bulb contacts water surface, replenishing water in the air-laid paper. It then rotates back to the initial position. As liquid ethanol in the bottom bulb is heated by ambient air and water evaporation keeps cooling down the top bulb, the device maintains this intermittent angular oscillating behavior. Please note that the self-floating design makes the device easy to deploy on natural water surface (e.g., lake and ocean) and ensures low friction during rotation.

The rotation dynamics were analyzed by extracting the time-resolved angles from recorded videos (Supplementary Video 1). As shown in Fig. 1(e), the device firstly rotates slowly and then the motion accelerates, which is clearly evidenced by the angular velocity shown in Fig. 1(f). This is because as the device rotates, the moment arm, i.e., distance between the gravitational center and the axis of rotation, also increases, producing an increasing torque. Once the "beak" on the top bulb contacts with water, the device oscillates with small amplitudes and then rotates back. Representative snapshots at different instants are also inserted in Fig. 1(d). It is interesting to note that, though the rotation is solely driven by gentle natural evaporation, the maximum angular velocity obtained is as high as 150 °/s. This fast instantaneous rotation makes it feasible to drive water-droplet based electricity generation. In addition, higher ambient temperature leads to high angular velocity and frequency of the periodic rotation (Fig. S3 in the ESM). Though the frequency is not high (at once per minute level), we envision this type of evaporation-driven generator may find applications for low-power consumption sensors in remote areas that only require intermittent sensing and remain idle at the rest of the time. The design of the hybrid hydrovoltaic generator and main energy conversion pathways are illustrated in Figs. 1(g) and 1(h). Thermal energy from the ambient air is converted to mechanical energy via the "evaporation motor". Mechanical energy is then converted to electricity in the droplet-electricity device. Meanwhile, this mechanical energy facilitates water-evaporation-induced electricity generation in the water-film mode. In the next sections, we first investigate the standalone evaporation-electricity and water-electricity devices under simulated working conditions, and then demonstrate the feasibility of the hybrid generator driven by natural evaporation.

2.2 Water evaporation induced electricity under water film mode

In the conventional one-end-immersing mode, i.e., a device with

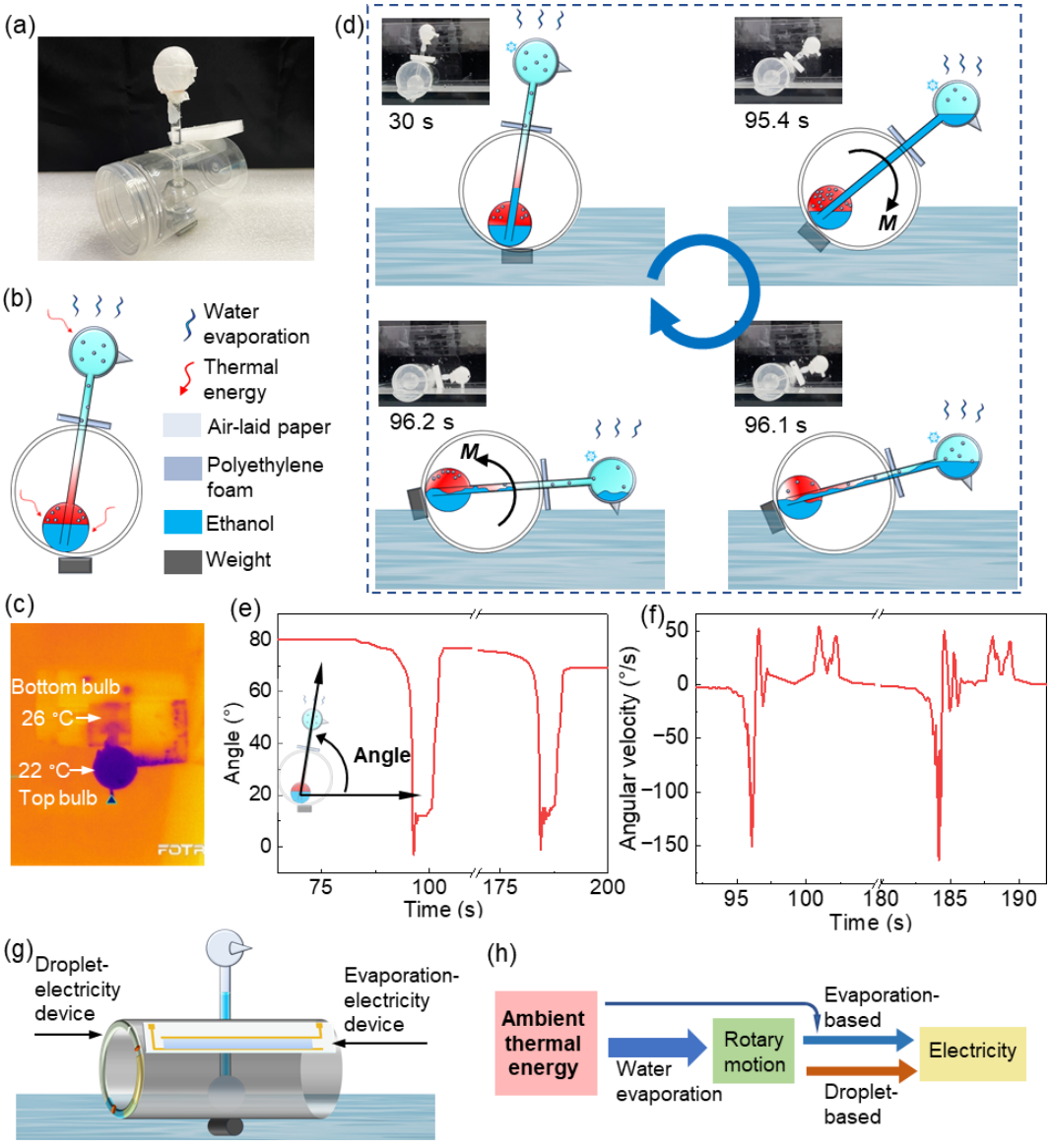

Figure 1 Working mechanism of the "evaporation motor". (a) Photo and (b) schematic diagram of the "evaporation motor". (c) Temperature of the top and bottom bulbs. The unit was floating on water and air-laid paper on the top bulb was wetted by water. (d) Schematic diagram of the working mechanism. Inserted photos were extracted from the recorded video at corresponding instants. (e) Time-resolved angle and (f) angular velocity of the "evaporation motor" during evaporation drive rotation. (g) Illustration of the proposed hybrid hydrovoltaic generator and (h) energy conversion pathways.

the bottom end of the porous film immersing in water, evaporation drives continuous imbibition of water into the nanoporous thin film and concurrent electricity generation [4]. However, the output voltage in this operation mode is generally limited to 1 volt, barely exceeding 3 volts [4–18]. In our previous work, we developed a water-film mode to broaden the capillary front, which was proven as the key region for electricity generation, and the obtained voltage output was almost one order of magnitude higher than that obtained under the one-end-immersing mode [24]. As shown in Fig. 2(a), the water-film mode involves intermittently inserting the device into and pulling it out from water in order to form a water film on the device (the experimental setup is displayed in Fig. S4 in the ESM). This is exactly what the "evaporation motor" does: by fixing the evaporation generator onto the cylindrical jar (Fig. 1(g)), the periodic rotation of the jar will perfectly enable the inserting and pulling motion. Therefore, it is beneficial to integrate the evaporation-electricity-generation device with the "evaporation motor".

The evaporation-electricity-generation device was fabricated by pasting a thin layer consisting of bismuth oxyhalide (BiOCl) nanoplates on an acrylic substrate with patterned Au electrode (Fig. 2(b)) [24, 42]. The BiOCl nanoplates are stacked irregularly, producing abundant micro- and nanopores. After the device is inserted into and pulled out from deionized water, a thin water film is formed on the BiOCl layer. With evaporation thinning and gravity dragging, the water film turns into a wedge shape, which broadens the capillary front and augments voltage output [24]. As shown in Figs. 2(c) and 2(d), along with water drying from the top, a visible wet edge (denoted by red dots) moves downward, creating a capillary front transitioning from the bottom wet region to the top dry region. As the wet edge keeps moving downward, the capillary front is further broadened. Therefore, the output voltage rises up concurrently until reaching a plateau as high as 4.3 V. This output voltage, benefiting from the water-film mode, is much higher than those obtained under the conditional one-end-immersing mode [4–18]. The effects of NaCl concentration in water is shown in Fig. S5 in the ESM. The output voltage decreases

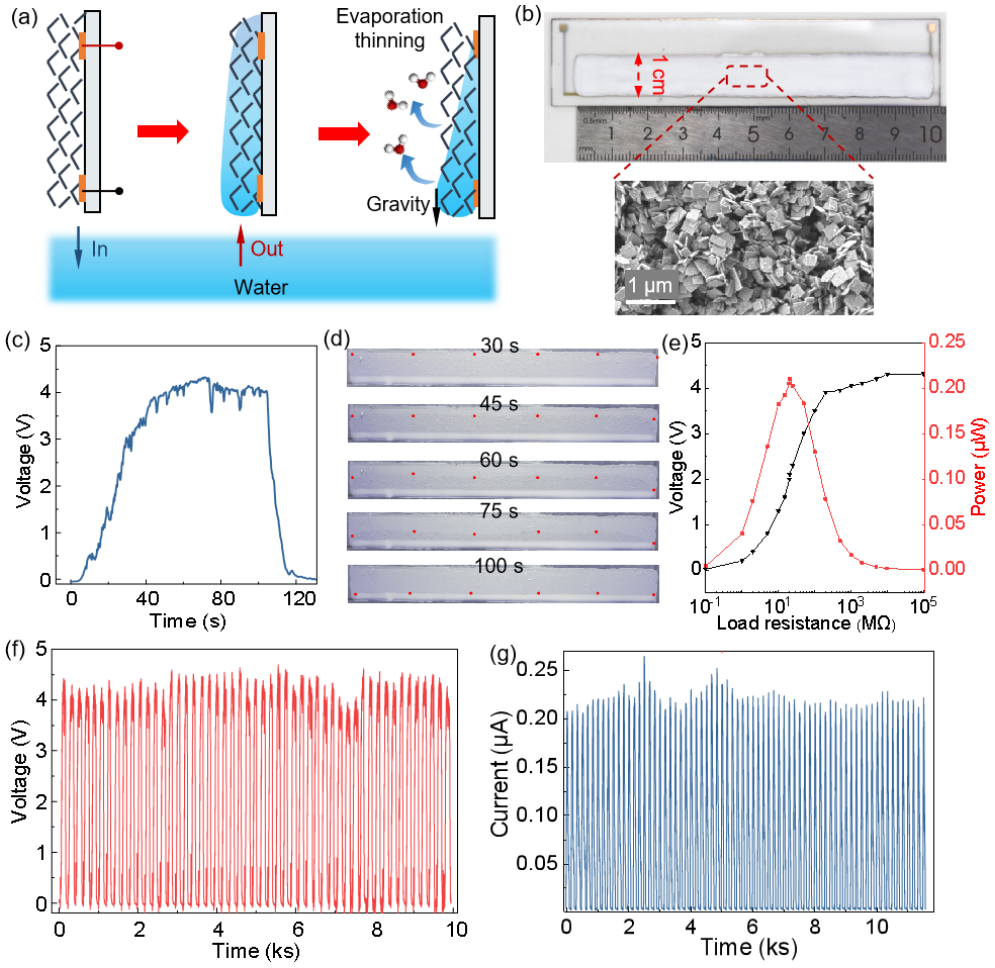

Figure 2 Performance of the standalone evaporation-electricity device. (a) Illustration of the water-film operation mode. (b) Photo of the device; insert is a SEM image of the BiOCl layer. (c) Representative voltage profile and (d) photos showing the wet edge position at corresponding instants; red dots denote position of the wet edge. (e) Voltage and power output with different load resistance. (f) Cycling voltage output and (g) current output.

with increasing the salt concentration (NaCl) because of the suppressed Debye length in the electrical double layer and reduced ionic selectivity in the nanochannels. The output current firstly increases because of the lowered internal resistance in salt solution, and then decreases at high salt concentration due to reduced ionic selectivity in the nanochannels.

To investigate the maximum power output, the load resistance (R) was varied from 0.1 Ω to 100 MΩ and the potential drop (V_R) on the resistance was recorded. Corresponding power output was then calculated by $P = V_R^2/R$. As exhibited in Fig. 2(e), the voltage output increases with increasing the load resistance, and the maximum power output, 0.21 μW, is achieved on a load resistance of 20.5 MΩ. This is micro-Watt level output could be further scaled up by device integration to provide on-demand power supply for electronics [24]. To demonstrate the durability of the device under the water-film mode, cycling tests were performed for 10 ks. As displayed in Figs. 2(f) and 2(g), the open-circuit voltage and short-circuit current maintain at about 4.3 V and 0.22 μA, respectively, with subtle fluctuations, indicating the device has great robustness and potential for long-term applications.

2.3 Rotational motion driven water droplet-based electricity generation

Water droplet spreading or sliding on dielectric layers, together with well-configured electrodes, can output electricity through electrostatic induction, thus converting mechanical energy into electricity [28–33]. In this work, to exploit the rotary motion of the "evaporation motor", we designed a water-droplet based generator, where a water column was encapsuled in a concentric annular FEP tube (Fig. 3(a)). As the device rotates with the "evaporation motor", the water column slides inside the tube recurringly. The two-drain-electrode configuration was adapted to efficiently collect and release electrostatically induced charges from this recurring motion [32]. A stepper motor was used to simulate the rotary motion (Fig. S6 in the ESM).

The electricity generation mechanism is illustrated in Fig. 3(a) and voltage and current output are displayed in Fig. 3(b). Initially, the water column stays at the left side of the source electrode (copper tape) covered region and conductively connects with the Drain-I electrode. As the tube rotates clockwise, the water column slides inside the tube because gravitational force overcomes friction. During this period, electrostatically-induced positive charges on the source gradually transfer to water through drain-I, which ceases once the water column detaches from Drain-I. As rotation proceeds, the water column contacts with the right drain-II, switching on the circuit and initiating quick transfer of positive charges from source to water via drain-II, producing high negative voltage and current pulses (Fig. 3(b)). Following this, the tube rotates counter-clockwise to the initial position and the water column detaches from drain-II, leaving charges accumulated in the water column. Once the water column contacts with the left

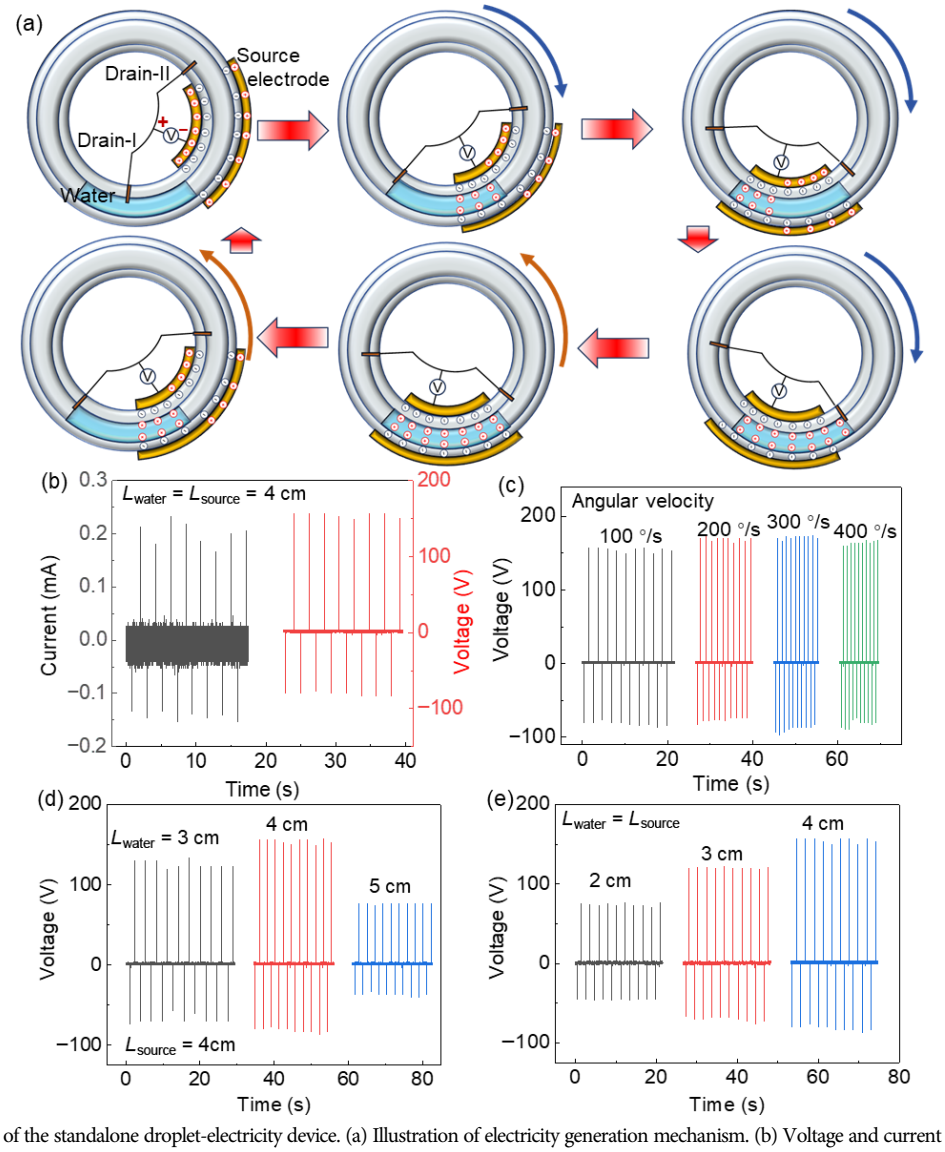

Figure 3 Performance of the standalone droplet-electricity device. (a) Illustration of electricity generation mechanism. (b) Voltage and current output. Voltage output with different (c) angular velocity, (d) water column length, and (e) source electrode length (same as the water column length).

drain-I again, the accumulated charges transfer back to source, inducing high positive voltage and current pulses (Fig. 3(b)). Therefore, the unit restores the water column position and charge distribution at the end of one cycle. While the rotation speed is relatively low (100 °/s), the current peak reaches as high as 0.2 mA and voltage as high as 150 V, implying high energy harvesting efficiency of the designed unit. The corresponding energy output in each cycle is about 0.1 μJ (Fig. S7 in the ESM).

The effects of rotation dynamics and unit configuration on voltage output are investigated. First, as shown in Fig. 3(c), the peak voltage does not change much when the rotation angular velocity increases from 100 to 400 °/s. This is because the sliding velocity of the water column relative to the tube has an upper limit set by friction, i.e., further increasing rotation speed exceeding 100 °/s does not lead to faster sliding of the water column. Second, the peak voltage is the highest when the source electrode and water column have the same length (Fig. 3(d)), which is consistent with previous reports [31, 32]. This can be explained as follows. A water column shorter than the source electrode results in smaller water-solid interface and thus less charge transfer; a water column longer than the source electrode results in longer overlapping area between the water column and source electrode when water contacts with drain-II (when rotating clockwise) and drain-I (when rotating counter-clockwise), reducing instantaneous charge transfer. Third, peak voltage increases with increasing the length of the source electrode and water column (Fig. 3(e)), because a longer source electrode contributes to larger water-solid interface for electrostatic induction. This implies the unit can be facilely scaled up by elongating the source electrode and water column. Based on these results and considering the size of the "evaporation motor", a source electrode and water column of 4 cm are used in the hybrid hydrovoltaic generator, investigated in the next section.

2.4 Hybrid hydrovoltaic electricity generation solely driven by natural water evaporation

After verifying that the standalone parts (evaporation-driven rotation, evaporation- and water-droplet-induced electricity) function as desired separately, we loaded the electricity generation devices onto the "evaporation motor" to obtain the hybrid hydrovoltaic generator, which is displayed in Fig. 4(a). We firstly confirmed that the hybrid generator could rotate driven by water evaporation and the period is about 64 s (Supplementary Video 2). With this rotary motion, the evaporation-electricity device was

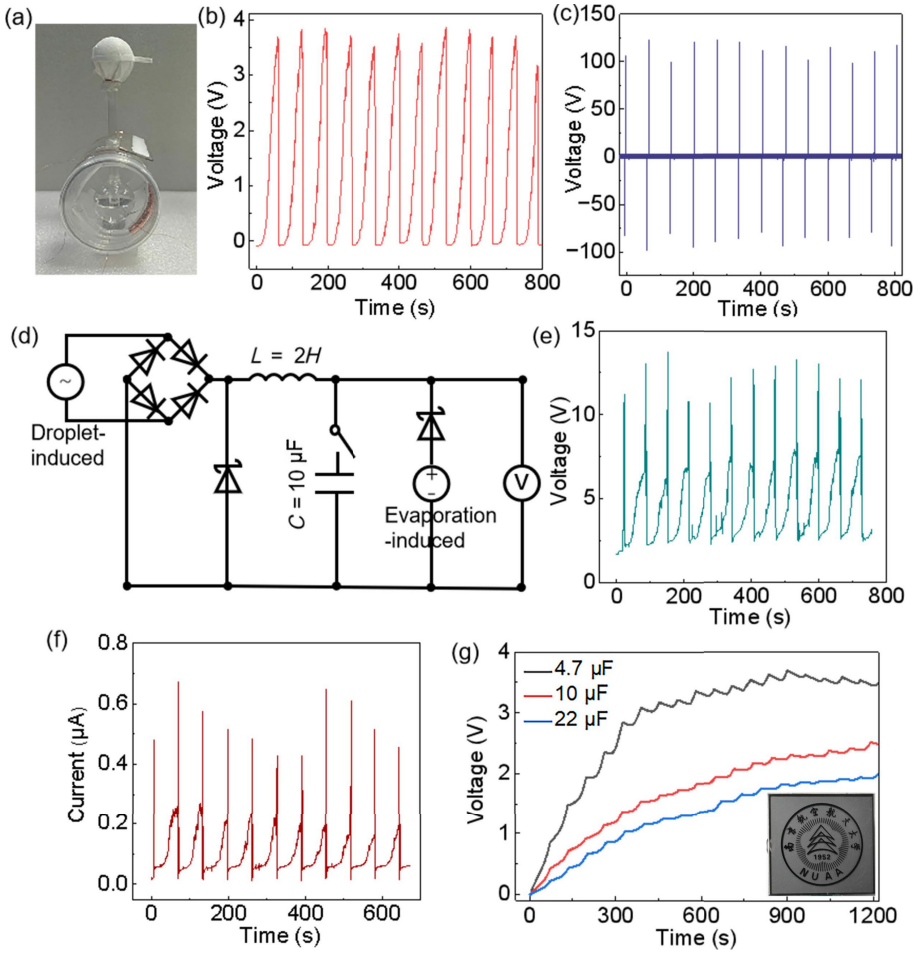

Figure 4 Performance of the hybrid hydrovoltaic generator. (a) Photo of the hybrid generator. Voltage output of the (b) evaporation-electricity and (c) droplet-electricity devices in the hybrid generator. (d) Diagram of the power management circuits. (e) Integrated voltage and (f) current output of the hybrid generator. (g) Charging curves of the capacitors; insert is a liquid crystal display powered by the capacitor (10 μF) charged by the integrated output.

immersed into and pulled out from water, making it work under the water-film mode that can efficiently induce electricity from water evaporation. As shown in Fig. 4(b), the obtained output peak voltage is ~3.8 V. The rotary motion also leads to the water column sliding inside the tube, producing a peak voltage of ~110 V (Fig. 4(c)). These results are similar to what obtained from the standalone devices working separately.

In order to integrate the power output from the evaporation and water-droplet devices, power management circuits (Fig. 4(d) and Fig. S8 in the ESM) were adopted [29]. Since the droplet device output has two pulses in each cycle with opposite polarities, a full-wave bridge rectifier is used to realize AC to DC conversion with high efficiency. An inductor of 2 H is used to capture energy from the high-peak but fort-duration pulses. The evaporation-electricity device is connected in parallel with the output of the power management circuits and a diode is added to eliminate current flow back. The integrated output voltage and current are exhibited in Figs. 4(e) and 4(f). It can be seen that the output from the evaporation-electricity device is similar to that shown in Fig. 4(b). The output of the droplet-electricity device, i.e., pulses with a peak of ~110 V, becomes pulses with DC tail components. The DC components are reflected as baseline shifts of ~2.1 V in Fig. 4(e) and ~50 nA in Fig. 4(f). This is because the inductor absorbs part of the pulse energy and the slowly releases it. Overall, the outputs of the evaporation-electricity device and droplet-electricity device are appropriately integrated to deliver augmented output.

To demonstrate potential applications of the hybrid hydrovoltaic generator, three capacitors are charged by the integrated output, respectively, and the voltage evolution curves are shown in Fig. 4(g). The 4.7 μF capacitor was charged to 3 V in 400 s; the 10 and 22 μF capacitors were charged to about 2.5 and 2 V in 1240 s, respectively. The stored energy in the 10 μF capacitor then successfully powered on a liquid crystal display (insert in Fig. 4(g)). Benefiting from the omnipresent nature of water evaporation, our device is subject to less restrictions from surrounding environments and weather and would find more widespread potential applications.

3 Conclusions

As different types of hydrovoltaic devices require distinctive stimuli, it is challenging to make them work simultaneously, especially under one single driving force. In this work, with the integration of an evaporation-dependent heat engine with two types of hydrovoltaic devices based on evaporation and water droplet, we for the first time developed a hybrid hydrovoltaic generator that is solely driven by water evaporation. The self-floating design makes it of low rotation resistance and easy to deploy. The induced recurring rotary motion propels water droplet to slide in a dielectric tube and produce pulse output ~100 V and ~0.2 mA. Meanwhile, rotary motion enables the evaporation-electricity device to work under a beneficial water-film operation mode that we recently developed to generate output of ~4 V and

~0.2 μA. Potential applications were demonstrated by charging capacitors by the integrated output and power electronics. This work paves the way for developing hybrid hydrovoltaic generators and further advancing hydrovoltaic technologies.

Acknowledgements

This work was supported by the National Natural Science Foundation of China (Nos. T2293691, 12172176, 12272181, 12311530052, and 12150002), the National Key Research and Development Program of China (No. 2019YFA0705400), Natural Science Foundation of Jiangsu Province (Nos. BK20220074, BK20211191, and BK20212008), the Research Fund of State Key Laboratory of Mechanics and Control for Aerospace Structures (MCMS-I-0421G01 and MCMS-I-0422K01), the Fundamental Research Funds for the Central Universities (NE2023003, NC2023001, NJ2023002, and NJ2022002) and the Fund of Prospective Layout of Scientific Research for NUAA (Nanjing University of Aeronautics and Astronautics).

Electronic Supplementary Material: Supplementary material (device fabrication, standalone tests of the evaporation-electricity devices and water-droplet-electricity devices, test of the hybrid hydrovoltaic generator, videos of periodic rotation of the "evaporation motor" and hybrid hydrovoltaic generator) is available in the online version of this article at https://doi.org/10.26599/NRE.2024.9120110.

Declaration of conflicting interests

The authors declare no conflicting interests regarding the content of this article.

Data availability

All data needed to support the conclusions in the paper are presented in the manuscript and/or the Supplementary Materials. Additional data related to this paper may be requested from the corresponding author upon request.

References

[1] Yin, J.; Zhou, J. X.; Fang, S. M.; Guo, W. L. Hydrovoltaic energy on the way. *Joule* **2020**, *4*, 1852–1855.

[2] Wang, X. F.; Lin, F. R.; Wang, X.; Fang, S. M.; Tan, J.; Chu, W. C.; Rong, R.; Yin, J.; Zhang, Z. H.; Liu, Y. P. et al. Hydrovoltaic technology: From mechanism to applications. *Chem. Soc. Rev.* **2022**, *51*, 4902–4927.

[3] Zhang, Z. H.; Li, X. M.; Yin, J.; Xu, Y.; Fei, W. W.; Xue, M. M.; Wang, Q.; Zhou, J. X.; Guo, W. L. Emerging hydrovoltaic technology. *Nat. Nanotechnol.* **2018**, *13*, 1109–1119.

[4] Xue, G. B.; Xu, Y.; Ding, T. P.; Li, J.; Yin, J.; Fei, W. W.; Cao, Y. Z.; Yu, J.; Yuan, L. Y.; Gong, L. et al. Water-evaporation-induced electricity with nanostructured carbon materials. *Nat. Nanotechnol.* **2017**, *12*, 317–321.

[5] Tan, J.; Fang, S. M.; Zhang, Z. H.; Yin, J.; Li, L. X.; Wang, X.; Guo, W. L. Self-sustained electricity generator driven by the compatible integration of ambient moisture adsorption and evaporation. *Nat. Commun.* **2022**, *13*, 3643.

[6] Fang, S. M.; Li, J. D.; Xu, Y.; Shen, C.; Guo, W. L. Evaporating potential. *Joule* **2022**, *6*, 690–701.

[7] Van Der Heyden, F. H. J.; Bonthuis, D. J.; Stein, D.; Meyer, C.; Dekker, C. Electrokinetic energy conversion efficiency in nanofluidic channels. *Nano Lett.* **2006**, *6*, 2232–2237.

[8] Wang, Z. Y.; Wu, Y. L.; Xu, K. Q.; Jiang, L. P.; Sun, J. K.; Cai, G. Y.; Li, G. F.; Xia, B. Y.; Liu, H. F. Hierarchical oriented metal-organic frameworks assemblies for water-evaporation induced electricity generation. *Adv. Funct. Mater.* **2021**, *31*, 2104732.

[9] Shao, B. B.; Wu, Y. F.; Song, Z. H.; Yang, H. W.; Chen, X.; Zou, Y. T.; Zang, J. Q.; Yang, F.; Song, T.; Wang, Y. S. et al. Freestanding silicon nanowires mesh for efficient electricity generation from evaporation-induced water capillary flow. *Nano Energy* **2022**, *94*, 106917.

[10] Liu, X. M.; Ueki, T.; Gao, H. Y.; Woodard, T. L.; Nevin, K. P.; Fu, T. D.; Fu, S.; Sun, L.; Lovley, D. R.; Yao, J. Microbial biofilms for electricity generation from water evaporation and power to wearables. *Nat. Commun.* **2022**, *13*, 4369.

[11] Tabrizizadeh, T.; Wang, J.; Kumar, R.; Chaurasia, S.; Stamplecoskie, K.; Liu, G. J. Water-evaporation-induced electric generator built from carbonized electrospun polyacrylonitrile nanofiber mats. *ACS Appl. Mater. Interfaces* **2021**, *13*, 50900–50910.

[12] Qin, Y. S.; Wang, Y. S.; Sun, X. Y.; Li, Y. J.; Xu, H.; Tan, Y. S.; Li, Y.; Song, T.; Sun, B. Q. Constant electricity generation in nanostructured silicon by evaporation-driven water flow. *Angew. Chem.* **2020**, *132*, 10706–10712.

[13] Shao, B. B.; Song, Z. H.; Chen, X.; Wu, Y. F.; Li, Y. J.; Song, C. C.; Yang, F.; Song, T.; Wang, Y. S.; Lee, S. T. et al. Bioinspired hierarchical nanofabric electrode for silicon hydrovoltaic device with record power output. *ACS Nano* **2021**, *15*, 7472–7481.

[14] Hu, Q. C.; Ma, Y. J.; Ren, G. P.; Zhang, B. T.; Zhou, S. G. Water evaporation-induced electricity with *Geobacter sulfurreducens* biofilms. *Sci. Adv.* **2022**, *8*, eabm8047.

[15] Zhang, G.; Duan, Z.; Qi, X.; Xu, Y. T.; Li, L.; Ma, W. G.; Zhang, H.; Liu, C. H.; Yao, W. Harvesting environment energy from water-evaporation over free-standing graphene oxide sponges. *Carbon* **2019**, *148*, 1–8.

[16] Ma, Q. L.; He, Q. Y.; Yin, P. F.; Cheng, H. F.; Cui, X. Y.; Yun, Q. B.; Zhang, H. Rational design of MOF-based hybrid nanomaterials for directly harvesting electric energy from water evaporation. *Adv. Mater.* **2020**, *32*, 2003720.

[17] Shao, C. X.; Ji, B. X.; Xu, T.; Gao, J.; Gao, X.; Xiao, Y. K.; Zhao, Y.; Chen, N.; Jiang, L.; Qu, L. T. Large-scale production of flexible, high-voltage hydroelectric films based on solid oxides. *ACS Appl. Mater. Interfaces* **2019**, *11*, 30927–30935.

[18] Li, L. H.; Zheng, Z.; Ge, C. L.; Wang, Y. F.; Dai, H.; Li, L. L.; Wang, S. Q.; Gao, Q.; Liu, M. Y.; Sun, F. Q. A flexible tough hydrovoltaic coating for wearable sensing electronics. *Adv. Mater.* **2023**, *35*, 2304099.

[19] Li, J. D.; Sheng, H.; Long, Y. Y.; Zhu, Y. L.; Deng, W.; Li, X. M.; Yin, J.; Guo, W. L. Passive gate-tunable kinetic photovoltage along semiconductor-water interfaces. *Angew. Chem., Int. Ed.* **2023**, *62*, e202218393.

[20] Tian, B. K.; Jiang, X. F.; Chu, W. C.; Zheng, C. X.; Guo, W. L.; Zhang, Z. H. Integrating reduced graphene oxides and PPy nanoparticles for enhanced electricity from water evaporation. *Int. J. Smart Nano Mater.* **2023**, *14*, 230–242.

[21] Li, J.; Liu, K.; Ding, T. P.; Yang, P. H.; Duan, J. J.; Zhou, J. Surface functional modification boosts the output of an evaporation-driven water flow nanogenerator. *Nano Energy* **2019**, *58*, 797–802.

[22] Li, L. H.; Feng, S. J.; Bai, Y. Y.; Yang, X. Q.; Liu, M. Y.; Hao, M. M.; Wang, S. Q.; Wu, Y.; Sun, F. Q.; Liu, Z. et al. Enhancing hydrovoltaic power generation through heat conduction effects. *Nat. Commun.* **2022**, *13*, 1043.

[23] Fang, S. M.; Chu, W. C.; Tan, J.; Guo, W. L. The mechanism for solar irradiation enhanced evaporation and electricity generation. *Nano Energy* **2022**, *101*, 107605.

[24] Deng, W.; Feng, G.; Li, L. X.; Wang, X.; Lu, H.; Li, X. M.; Li, J. D.; Guo, W. L.; Yin, J. Capillary front broadening for water-evaporation-induced electricity of one kilovolt. *Energy Environ. Sci.* **2023**, *16*, 4442–4452.

[25] Yin, J.; Li, X. M.; Yu, J.; Zhang, Z. H.; Zhou, J. X.; Guo, W. L.

Generating electricity by moving a droplet of ionic liquid along graphene. *Nat. Nanotechnol.* **2014**, *9*, 378–383.

[26] Yin, J.; Zhang, Z. H.; Li, X. M.; Yu, J.; Zhou, J. X.; Chen, Y. Q.; Guo, W. L. Waving potential in graphene. *Nat. Commun.* **2014**, *5*, 3582.

[27] Yang, S. S.; Su, Y. D.; Xu, Y.; Wu, Q.; Zhang, Y. B.; Raschke, M. B.; Ren, M. X.; Chen, Y.; Wang, J. L.; Guo, W. L. et al. Mechanism of electric power generation from ionic droplet motion on polymer supported graphene. *J. Am. Chem. Soc.* **2018**, *140*, 13746–13752.

[28] Xu, W. H.; Zheng, H. X.; Liu, Y.; Zhou, X. F.; Zhang, C.; Song, Y. X.; Deng, X.; Leung, M.; Yang, Z. B.; Xu, R. X. et al. A droplet-based electricity generator with high instantaneous power density. *Nature* **2020**, *578*, 392–396.

[29] Li, X. M.; Ning, X. Y.; Li, L. X.; Wang, X.; Li, B. W.; Li, J. D.; Yin, J.; Guo, W. L. Performance and power management of droplets-based electricity generators. *Nano Energy* **2022**, *92*, 106705.

[30] Li, L. X.; Wang, X.; Deng, W.; Yin, J.; Li, X. M.; Guo, W. L. Hydrovoltaic energy from water droplets: Device configurations, mechanisms, and applications. *Droplet* **2023**, *2*, e77.

[31] Li, L. X.; Li, X. M.; Yu, X.; Shen, C.; Wang, X.; Li, B. W.; Li, J. D.; Wang, L. F.; Yin, J.; Guo, W. L. Boosting the output of bottom-electrode droplets energy harvester by a branched electrode. *Nano Energy* **2022**, *95*, 107024.

[32] Zheng, H. X.; Wu, H.; Yi, Z. R.; Song, Y. X.; Xu, W. H.; Yan, X. T.; Zhou, X. F.; Wang, S.; Wang, Z. K. Remote-controlled droplet chains-based electricity generators. *Adv. Energy Mater.* **2023**, *13*, 2203825.

[33] Wei, X. L.; Zhao, Z. H.; Zhang, C. G.; Yuan, W.; Wu, Z. Y.; Wang, J.; Wang, Z. L. All-weather droplet-based triboelectric nanogenerator for wave energy harvesting. *ACS Nano* **2021**, *15*, 13200–13208.

[34] Zhang, N.; Gu, H. J.; Zheng, H. X.; Ye, S. M.; Kang, L.; Huang, C.; Lu, K. Y.; Xu, W. H.; Miao, Q. Q.; Wang, Z. K. et al. Boosting the output performance of volume effect electricity generator (VEEG) with water column. *Nano Energy* **2020**, *73*, 104748.

[35] Wang, X.; Fang, S. M.; Tan, J.; Hu, T.; Chu, W. C.; Yin, J.; Zhou, J. X.; Guo, W. L. Dynamics for droplet-based electricity generators. *Nano Energy* **2021**, *80*, 105558.

[36] Cheedarala, R. K.; Song, J. I. Sand-polished Kapton film and aluminum as source of electron transfer triboelectric nanogenerator through vertical contact separation mode. *Int. J. Smart Nano Mater.* **2020**, *11*, 38–46.

[37] Xu, T.; Ding, X. T.; Cheng, H. H.; Han, G. Y.; Qu, L. T. Moisture-enabled electricity from hygroscopic materials: A new type of clean energy. *Adv. Mater.* **2023**, 2209661.

[38] Zhao, F.; Liang, Y.; Cheng, H. H.; Jiang, L.; Qu, L. T. Highly efficient moisture-enabled electricity generation from graphene oxide frameworks. *Energy Environ. Sci.* **2016**, *9*, 912–916.

[39] Wang, H. Y.; Sun, Y. L.; He, T. C.; Huang, Y. X.; Cheng, H. H.; Li, C.; Xie, D.; Yang, P. F.; Zhang, Y. F.; Qu, L. T. Bilayer of polyelectrolyte films for spontaneous power generation in air up to an integrated 1,000 V output. *Nat. Nanotechnol.* **2021**, *16*, 811–819.

[40] Liu, X. M.; Gao, H. Y.; Ward, J. E.; Liu, X. R.; Yin, B.; Fu, T. D.; Chen, J. H.; Lovley, D. R.; Yao, J. Power generation from ambient humidity using protein nanowires. *Nature* **2020**, *578*, 550–554.

[41] Xu, T.; Ding, X. T.; Huang, Y. X.; Shao, C. X.; Song, L.; Gao, X.; Zhang, Z. P.; Qu, L. T. An efficient polymer moist-electric generator. *Energy Environ. Sci.* **2019**, *12*, 972–978.

[42] Deng, W.; Li, Y. Novel superhydrophilic antifouling PVDF-BiOCl nanocomposite membranes fabricated via a modified blending-phase inversion method. *Sep. Purif. Technol.* **2021**, *254*, 117656.

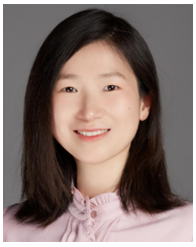

Xuemei Li received her PhD degree in 2016 for the thesis on the synthesis and properties of two-dimensional materials. Now she is an associate professor at Nanjing University of Aeronautics and Astronautics (NUAA) and focuses on the physical mechanics of nano-materials.

Gu Feng is currently a postgraduate student at Institute of Nanoscience of Nanjing University of Aeronautics and Astronautics (NUAA), and is primarily focused on on energy conversion at solid–liquid interfaces.

Wei Deng obtained his PhD degree from Texas A&M University (TAMU) in 2019, and worked as a visiting assistant professor in the Department of Mechanical Engineering from 2019 to 2021. He is currently an associate professor in the Institute for Frontier Science at NUAA, working on hydrovoltaic technology and advanced water treatment technologies.

Wanlin Guo obtained his PhD from Northwestern Polytechnical University in 1991, and was elected as an academician of the Chinese Academy of Science in 2017. He is a Chair Professor at NUAA and the founding director of the Key Laboratory of Intelligent Nano Materials and Devices of Ministry of Education. His research focuses on intelligent nano materials and devices, novel conception and technology for efficient energy conversion, molecular physical mechanics for neuronal signaling and molecular biomimics, as well as strength and safety of aircraft and engines.